Efficiency Improvement of Parallel Source Inverters in Islanded AC Microgrid

Md Akib Hasan
Faculty of Electrical Engineering and Technology
Universiti Malaysia Perlis
Perlis, Malaysia
hasan33-2718@diu.edu.bd

Md Showkot Hossain
Faculty of Electrical Technology and Engineering
Universiti Teknikal Malaysia Melaka
Melaka, Malaysia
hossain33-2682@diu.edu.bd

Mohd Azrik Roslan
Faculty of Electrical Engineering and Technology
Universiti Malaysia Perlis
Perlis, Malaysia
mazrik@unimap.edu.my

Azralmukmin Azmi
Faculty of Electrical Engireering and Technology
Universiti Malaysia Perlis
Perlis, Malaysia
azralmukmin@unimap.edu.my

Jenn Hwai Leong
Faculty of Electrical Engineering and Technology
Universiti Malaysia Perlis
Perlis, Malaysia
jhleong@unimap.edu.my

Ahmad Afif Nazib
Faculty of Electrical Engineering and Technology
Universiti Malaysia Perlis
Perlis, Malaysia
ahmadafif@unimap.edu.my

2024 IEEE International Conference on Power and Energy (PECon) | 979-8-3503-6197-1/24/$31.00 ©2024 IEEE | DOI: 10.1109/PECON62060.2024.10827539

***Abstract*— The limited capacity of a single inverter has led to the implementation of parallel inverters for interconnecting renewable energy generation systems. Droop control is commonly used for operating parallel inverters; however, conventional droop control has a low conversion efficiency under heavy loads. Therefore, this paper designed an efficient control strategy to enhance the conversion efficiency of parallel inverters. The employed method incorporates an internal current and voltage control loop based on a synchronous reference frame, along with conventional PI controllers. Additionally, Particle Swarm Optimization (PSO) is utilized to determine the optimal conversion efficiency of the parallel inverters. In this approach, the distributed generation (DG) unit adjusts its control mode to modify system voltage and frequency in response to dynamic load conditions. Efficiency improvements were observed in the range of 0.19% to 0.41% across various initial power distribution ratios, highlighting the efficacy of optimized droop parameters in maintaining robust and efficient power systems. Simulation results using MATLAB/SIMULINK demonstrate that the proposed control system improves system efficiency**

***Keywords*— microgrid, parallel inverters, droop control, particle swarm optimization (PSO), efficiency improvement**

I. Introduction

A microgrid generally includes local distributed generators (DGs), energy storage systems, and different thermal and electric loads. It works alongside the conventional power grid to handle rising load demands and can function in both grid-connected and islanded modes [1], [2].

Integrating of micro-sources like photovoltaics, wind turbines, hydropower, and fuel cells provides scalable green energy alternatives. These sources are often connected via Pulse Width Modulation Voltage Source Inverters (PWM-VSIs). The semiconductor components of these inverters exhibit non-linear voltage-current characteristics and operate at high switching frequencies, thereby enhancing power quality for end users [3], [4].

Achieving high efficiency, desired power quality, and seamless DG integration in microgrids requires a robust control system. The droop control technique is an essential component of PWM-VSIs systems, ensures accurate current compensation. Droop controllers like P-f and Q-V employ predictive control or Proportional Integral (PI), alongside Space Vector Pulse Width Modulation (SVPWM), enhancing performance with stable switching and minimal ripple [5].

Additionally, to produce PWM reference voltage signals, it is common practice to integrate a current control loop with an external power control loop. This solution employs a power control system that ensures satisfactory power quality. An active-reactive power monitoring technique is employed during network connection mode. However, when operating in island mode, a voltage-frequency control approach is implemented. Based on these circumstances, the DG unit is required to deliver the highest possible power production while ensuring the stability of the system [6]. Recent studies [7], [8], [9] have applied power control strategies to microgrids, facilitating analysis and comparison. However, despite considerations for dynamic performance, load sharing, and controller specifics, these approaches lack automatic parameter adjustment mechanisms necessary for optimizing performance during rapid system changes.

Microgrid operation relies on DG units with low power output, necessitating cooperation among several units for frequency control. However, DGs like solar and wind cells cannot contribute due to their uncertain output [10]. Therefore, a voltage source inverter (VSI) serves as a reference for voltage and frequency, with storage employed for frequency compensation. The VSI's performance is governed by its droop characteristic, wherein more power is injected into the microgrid as frequency drops, compensating for load changes [11]. Secondary frequency control requires adjusting the no-load frequency upwards in the droop method, typically using a proportional integral (PI) controller [12].

Artificial intelligence (AI) algorithms have become essential in the power system, offering unparalleled advantages in control, modelling, operation, and analysis, replacing traditional methods and becoming the primary solution approach [13]. In [14], utilized the consistency algorithm and genetic algorithm (GA) to optimize the characteristics of a microgrid. This optimization led to enhanced dynamic performance and provided guidance for the design of droop control in low voltage microgrids. However, neglecting line impedance effects on DG and system power allocation was a limitation. In [15], [16] enhanced droop control parameter optimization using improved particle swarm optimization, enhancing microgrid power allocation

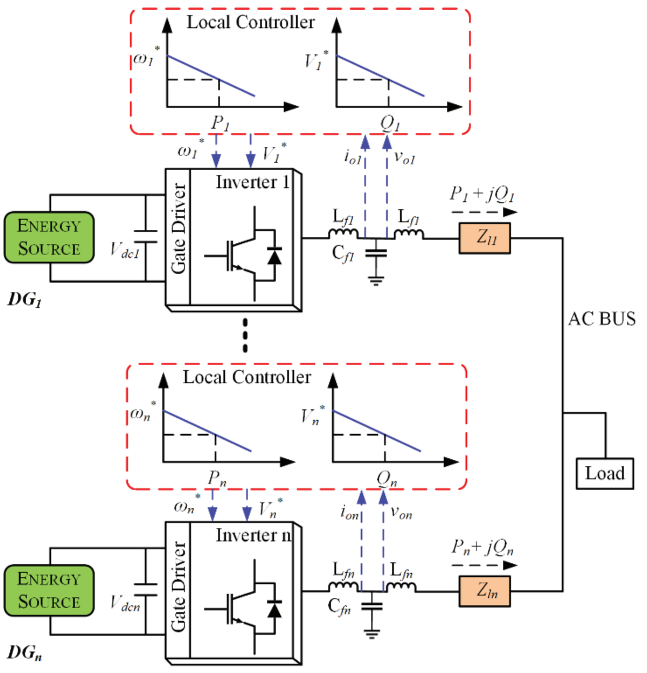

Fig. 1. The circuit configuration of islanded AC microgrid.

accuracy. Yet, centralized control structures increased system complexity and communication demands. Modifying the inertia weights and learning factors in the particle swarm optimization algorithm enhanced the convergence and search speed [17]. However, the issue of parameter diversity still remains a challenge.

Therefore, this article presents an optimized droop control approach that enhances the efficiency of microgrid operations without relying on communication facilities. The primary contributions are discussed as follows: (i) Initially examines the microgrid configuration and the impact of line parameters on conventional droop control. (ii) Design an efficient control strategy that enhances the conversion efficiency of parallel inverters. (iii) The PSO algorithm is utilized to determine the optimal conversion efficiency. Results from simulation conclusively show that the implemented droop control method enhances power allocation accuracy, stability and efficiency in microgrids.

The structure of this paper is as follows: Section II introduces system configuration, Section III details efficiency modelling and analysis for single bus AC microgrid, Section IV discusses optimization techniques. In Section V and VI, the optimization droop control strategy and simulation results are provided to validate the proposed control strategy. Conclusions are drawn in Section VII.

II. System Configuration

The circuit layout of an islanded microgrid with n-parallel inverters is shown in Fig. 1. This configuration employs a droop control technique to achieve proportional power distribution, which is determined by the power ratings of the inverters. Droop control strategies play a vital role in achieving proportional power distribution among the paralleled inverters in islanded microgrids. The traditional strategy for controlling active power-frequency (P-ω) and reactive power-voltage (Q-V) droop is represented by Eq. (1) and (2) [18].

$$\omega_c^* = \omega_o - m_c P_c \, , m_c = \frac{(\omega_{max} - \omega_{min})}{P_{max\_c}} \tag{1}$$

$$V_c^* = V_o - n_c Q_c \, , n_c = \frac{(V_{max} - V_{min})}{Q_{max\_c}} \tag{2}$$

where, ω_c^* and V_c^* are the reference commands for angular frequency and output voltage amplitude. P_c and Q_c denote the output active and reactive power of the c-th converter, while P_{max_c} and Q_{max_c} indicate its active and reactive power ratings. The no-load angular frequency and output voltage are ω_o and V_o. The coefficients m_c and n_c, based on power ratings, serve as droop coefficients. ω_{max} and ω_{min} define the allowable range for angular frequency, while V_{max} and V_{min} specify the upper and lower limits for voltage amplitude, respectively.

The power-sharing relationship among paralleled inverters can be determined from Eq. (1) and (2) as follows:

$$\begin{cases} m_1 P_1 = m_2 P_2 = \cdots = m_n P_n \\ n_1 Q_1 = n_2 Q_2 = \cdots = n_n Q_n \end{cases} \tag{3}$$

Eq. (3) shows that proportional power sharing is automatically achieved by the conventional droop control approach based on the defined droop coefficients. However, in an AC microgrid, this method fails to produce the highest efficiency when utilizing the specific power sharing ratio [19], [20].

III. Efficiency Assessment And Modelling For Single Bus AC Microgrid

This section presents an efficiency model for the microgrid and details the power loss calculation methodology for the inverter. The electrical conversion efficiency (η) of a converter is the ratio of output power (P_{out}) to input power (P_{in}), with the loss (P_{loss}) consumed by internal components. These losses are influenced by voltage, current, temperature, and device age. The PSO Method is used to optimize the efficiency model, determining optimal operating conditions.

A. Inverter Loss Analysis and Modelling

Fig. 2 illustrate the power flow of an inverter, indicating that inverter power loss is related to the electrical appliance and transmission cable. Each powered electronic module's loss specifications are based on its manufacturing characteristics, requiring manufacturer data and device datasheets for accurate calculations. To select appropriate power devices, it is necessary to estimate total inverter power losses. For a three-phase load, Eq. (4) [19] can be used to calculate the total power loss of the c-th converter.

$$P_{loss\_c} = a_c \cdot P_c^2 + b_c \cdot P_c + c_c \tag{4}$$

where P_c is the output power and a_c, b_c, c_c are represents the power loss coefficients of the c-th converter. Power loss coefficients of each inverter are calculated using PSIM simulation platform and then MATLAB curve fitting tools in fitted function by simulation data.

The parasitic resistance is the cause of the power loss in the transmission line, as represented in Eq. (5) [21].

$$P_{loss\_lc} = R_{lc} \, I_{RMS\_lc}^2 \tag{5}$$

where R_{lc} represents the parasitic resistance of the transmission line. I_{RMS_lc} represents the root mean square of current flowing through the transmission line. This value is

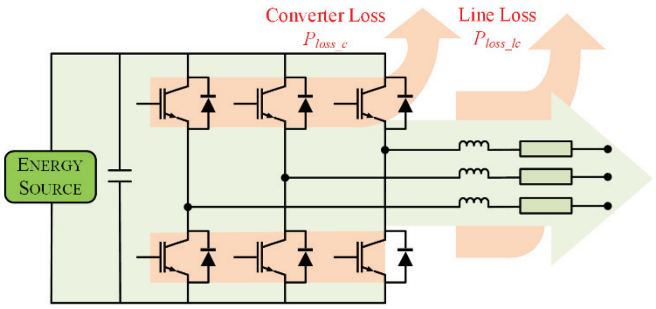

Fig. 2. Inverter power flow diagram in a microgrid.

determined by the network topology and can be calculated using Eq. (6).

$$I_{RMS\_lc} = I_{RMS\_c} = \frac{\sqrt{2}}{3\,V_m \cos\varphi} P_c = dP_c \tag{6}$$

Where V_m represents the amplitude of the output voltage. By combining Eq. (5) and (6), the relationship between power loss and output power can be expressed as Eq. (7).

$$P_{loss\_lc} = R_{lc}\, d^2 P_c^2 \tag{7}$$

Considering inverter and transmission line losses, the overall system power loss is provided by Eq. (8).

$$P_{loss\_total} = \sum_{c=1}^{N} P_{loss\_c} + \sum_{j=1}^{M} P_{loss\_lj} \tag{8}$$

Where N and M are the number of converters and transmission lines, respectively.

B. Inverter Efficiency Modelling for Single-bus Microgrid

A single-bus microgrid is analyzed to examine load location effects on efficiency. Fig. 3 depicts a microgrid configuration consisting of multiple inverters connected in parallel to a common bus. The system efficiency of a microgrid composed of N-paralleled inverters can be defined as follows [20]:

$$\eta_{sys} = \frac{P_{load}}{P_{in}} = \frac{P_{load}}{P_{load} + P_{loss\_total}} \tag{9}$$

where,

$$P_{loss\_total} = \sum_{c=1}^{N} P_{loss\_c} + \sum_{j=1}^{M} P_{loss\_lj} \tag{10}$$

To maximize system efficiency, the issue is to get optimal power distribution. Total power loss (P_{loss_total}) reduction is necessary to maximize system efficiency while the load demand is constant. Therefore, the optimization issue, without considering power ratings, could be expressed as Eq. (11).

$$\min(P_{loss\_total})$$
$$\left\{ \sum_{c=1}^{N} P_c = P_{load} + \sum_{c=1}^{N} P_{loss\_lc} \right. \tag{11}$$

During practical operation, the amount of power loss in cables is considerably lower than the amount of power needed by the load. The optimal power-sharing ratio determine by the inverter's distance from the common bus. Identical inverters share power equally due to equivalent loss characteristics, while different inverters' optimal power-sharing ratios depend on their loss characteristics [19].

The improved efficiency is defined as:

$$\eta_{imp} = \frac{\eta_{opt} - \eta_{con}}{\eta_{con}} \cdot 100\% \tag{12}$$

Where ere η_{con} and η_{opt} are efficiency under conventional and optimized droop control. Simulation results show the proposed control strategy improves overall efficiency across varying load profiles.

IV. Optimization Techniques

The PSO algorithm begins by initializing a set of random particles (random solutions) in order to search for the optimal solution through iterative processes. During the optimization process, particles undergo updates using two extreme values in each iteration: one is the optimal solution identified by the particle itself, known as the individual extremum; the other extreme value is determined by the entire population and is referred to as the global extremum [22].

In the target search space with d dimensions, there is a group of n particles. Once the two extreme values mentioned above are identified, the particles adjust their position and speed using the following formula [23]:

$$v_{id} = \omega \cdot v_{id} + c_1 r_1 (p_{id} - x_{id}) + c_2 r_2 (p_{gd} - x_{id}) \tag{13}$$

$$x_{id} = v_{id} + x_{id} \tag{14}$$

The variables c_1 and c_2 denote the learning factors, often referred to as acceleration constants. The variables r_1 and r_2 are random numbers uniformly distributed within the interval [0, 1]. The variable ω represents the inertia weight, which serves to preserve the particles motion inertia and enhance the exploration of the search space.

The fitness function of the algorithm for PSO is designed to minimize the total loss in the system, including both inverter losses and line losses. The fitness function is evaluated for each particle's position (set of droop coefficients), and the PSO algorithm iteratively updates the particles to determine the optimum solution that minimizes this fitness function.

The fitness function of the PSO algorithm is:

$$f(m_{p1}, m_{p2}, m_{p3}) = \sum_{c=1}^{3} P_{loss\_c} + \sum_{c=1}^{3} P_{loss\_lc} \tag{15}$$

Where P_{loss_c} and P_{loss_lc} are the inverters internal and transmission line losses of the c-th converter respectively.

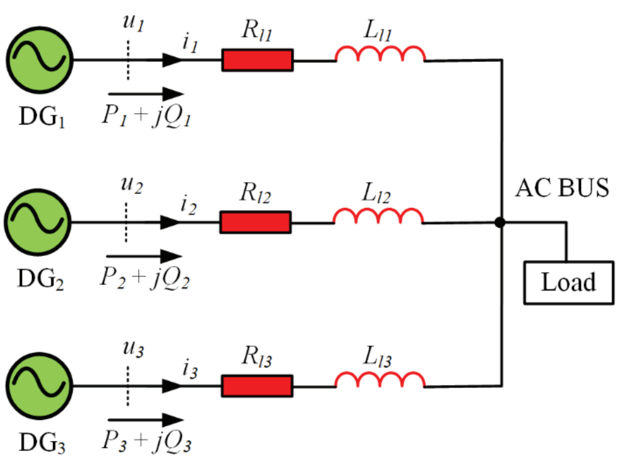

Fig. 3. Schematic of a single-bus microgrid configuration.

V. Optimized Droop Control Strategy

The flowchart of the PSO algorithm's optimized droop control, as formulated in this research, is illustrated in Fig. 4. This figure details the steps of the PSO algorithm employed to minimize total losses in an inverter system while considering line impedance. Fig. 5 illustrates the schematic of the droop controller that has been designed. The power loss coefficients for every converter are calculated using the PSIM simulation platform, utilizing the power loss estimation method described in Section III. Next, in order to achieve optimal power sharing, these coefficients are integrated into the optimized droop controller.

Within the microgrid, a DG unit operates, and the droop controller supplies control signals to its inverter. To enhance control efficiency and minimize computational demands, a local controller processes real-time data from each DG unit, subsequently updating the local inverter.

The calculation module generates variables for the PSO module, which iteratively optimizes control parameters. The extreme values derived from these iterations are fed into the droop control module, continuously updating the droop coefficients in real-time. The local controller recalculates power references every 0.5 seconds. When there are changes in load demand, the optimized droop controller adjusts the droop coefficients to maintain system stability. As illustrated in Fig. 1, the designed controller can operate without requiring a communication facility, thereby enhancing the dependability and adaptability of the control system.

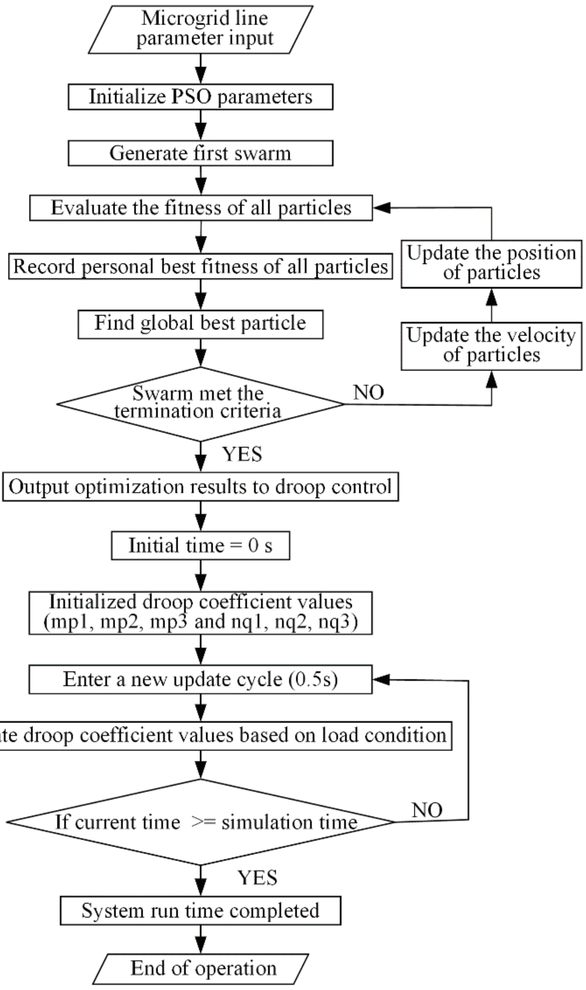

Fig. 4. System flowchart for optimized droop control.

VI. Simulation Results

To validate the effectiveness of the optimized droop control strategy, simulation verification was conducted using an AC microgrid with three parallel inverters in the MATLAB/Simulink platform. In this study, analyze the performance of an optimized droop control method under 0.8 and 0.85 power factor load condition at the bus bar, with the simulation run over a period of 1.5 seconds covering load profiles of 50%, 80%, and 100% of a total 130 kVA load.

The circuit configuration of this simulated AC microgrid is depicted in Fig. 1. Each inverter comprises a six-pack IGBT full-bridge power electronics component. System-level parameters used in the simulation are detailed in Table I. Comprehensive specifications for these power devices can be typically found in manufacturer datasheets [24], [25], [26].

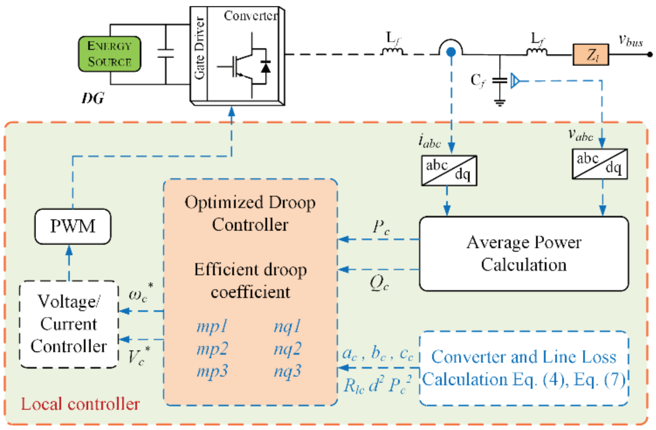

Fig. 5. Block diagram of the optimized droop controller.

TABLE I. System Parameters

Inverter Specifications			
Parameter	***Inverter 1***	***Inverter 2***	***Inverter 3***
Manufacturer	Powerex	Infineon	Infineon
Power device	CM100TU-12H	FS200R07PE4	FS225R12OE4
Power rating	30 kVA	40 kVA	60 kVA
DC voltage	V_{dc1} = 600V	V_{dc2} = 600V	V_{dc3} = 600V
Power loss coefficients	a_1 = 3.4e-7 b_1 = 1.36e-2 c_1 = 6.25e-1	a_2 = 7.25e-8 b_2 = 1.33e-2 c_2 = 6.14e1	a_3 = 5.22e-7 b_3 = 1.25e-2 c_3 = 2.18e2
Circuit and Control Parameters			
Filter parameters	L_{f1}=L_{f2}=L_{f3}=1.35mH C_{f1}=C_{f2}=C_{f3}=50μF L_{c1}=L_c=L_{c3}=0.35mH	Phase voltage frequency reference	$V_m^* = 325\ V$ $\omega^* = 100\pi\ rad/s$
Line impedance	Z_{l1}=(0.46+j0.53) Ω Z_{l2}=(0.33+j0.38) Ω Z_{l3}=(0.2+j0.23) Ω	Switching frequency	f_{sw1}=f_{sw2}=f_{sw3} = 10 kHz

A. *Case I: Power Factor 0.8*

The active power distribution among three units, P_1, P_2, and P_3, is compared between conventional and optimized droop control methods. Fig. 6 displays the simulation outcomes of three parallel inverters, each having distinct power ratings and power devices. The system capacity experiences time-varying load of 65 kVA, 104 kVA, and 130 kVA during the time intervals of 0-0.5s, 0.5-1.0s, and 1.0-1.5s. Fig. 6(a)-(b) illustrates the power sharing features of inverter1, inverter2 and inverter3. The optimized droop control strategy dynamically regulates the power sharing ratio to enhance system efficiency. The system efficiency under optimized droop and conventional droop control is shown in Fig. 6(c).

The efficiency improvement (η_{imp}) for the optimized method is 0.26% at 50% load, 0.38% at 80% load, and 0.26% at 100% load. The optimized droop control method achieves more stable and slightly more efficient power distribution compared to the conventional method, leading to significant energy savings and reduced operational costs over time, especially under varying load conditions. Thus, it demonstrates a clear advantage in maintaining higher system efficiency and balanced power distribution, making it a favorable approach for managing power in dynamic load systems.

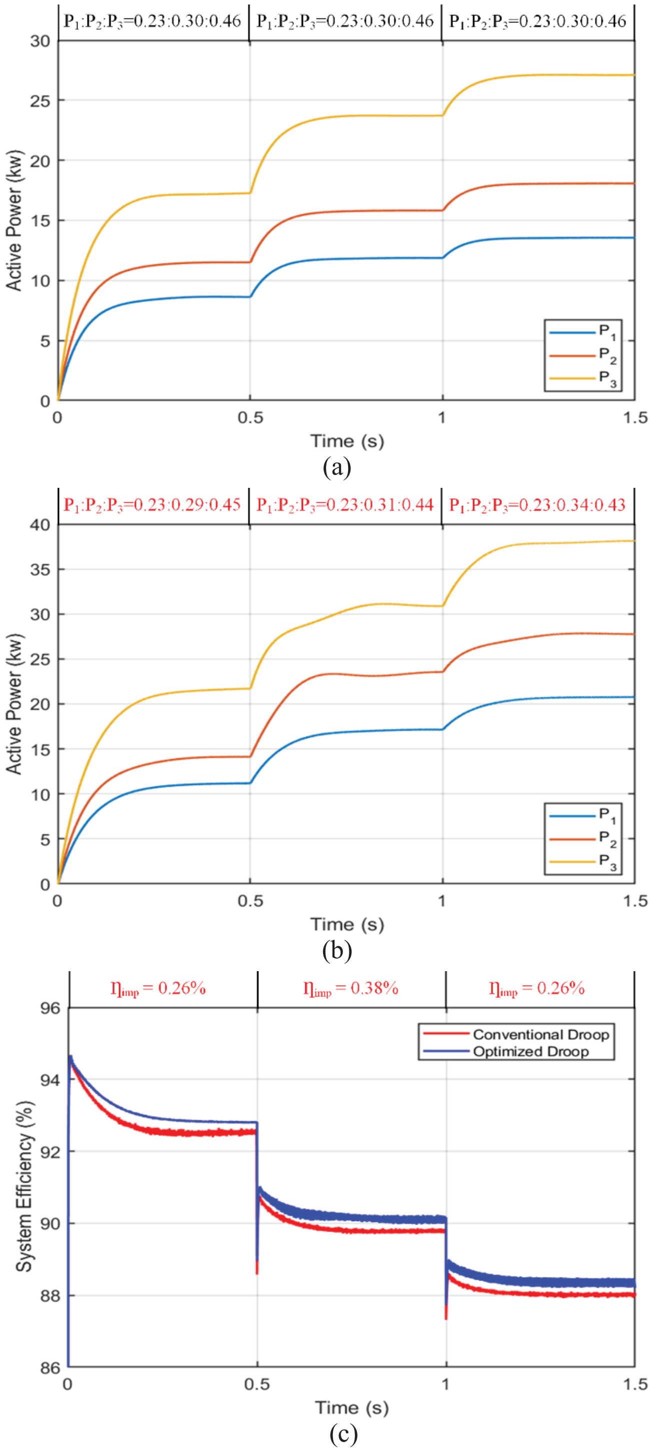

Fig. 6. Simulation results of case I. (a) Active power sharing under conventional droop control strategy. (b) Active power sharing under optimized droop control. (c) System efficiency under conventional and optimized droop control.

B. *Case II: Power Factor 0.85*

The active power distribution among three units, P_1, P_2, and P_3 is illustrated for both conventional and optimized droop control methods. Fig. 7 displays the simulation outcomes of three inverters that are connected in parallel. These inverters have varying power ratings and utilize different power devices. The system capacity undergoes time-varying load of 65 kVA, 104 kVA, and 130 kVA during the time intervals of 0-0.5s, 0.5-1.0s, and 1.0-1.5s, respectively. Fig. 7(a)-(b) illustrates the power sharing characteristics of inverter1, inverter2 and inverter3.

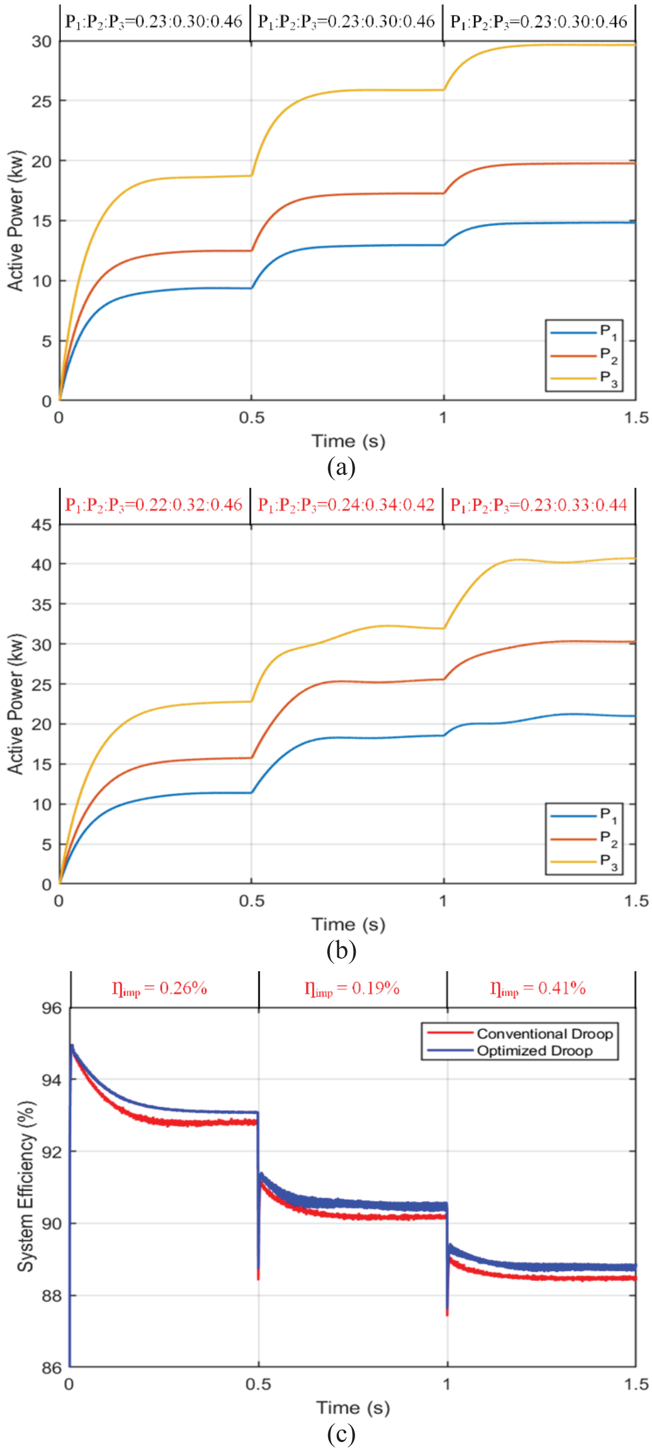

Fig. 7. Simulation results of case II. (a) Active power sharing under conventional droop control strategy. (b) Active power sharing under optimized droop control. (c) System efficiency under conventional and optimized droop control.

The optimized droop control strategy adaptively regulates the power sharing ratio to enhance system efficiency. Figure 7(c) presents a comparative analysis of the efficiency of the system using conventional droop control and optimized droop control. The efficiency improvement (η_{imp}) for the optimized method is 0.26% at 50% load, 0.19% at 80% load, and 0.41% at 100% load. The optimized droop control method exhibits a similar power distribution pattern but with a more balanced load distribution, reducing stress on individual units. Overall, the optimized droop control method provides a more stable and slightly more efficient power distribution compared to the conventional method. The marginal efficiency improvement can lead to significant energy savings and reduced operational costs over time.

VII. Conclusion

This paper presents an optimized droop controller designed to maximize the efficiency of parallel inverter systems while minimizing inverter and transmission losses. The algorithm optimizes the traditional droop coefficient in real time, enhancing system efficiency. Simulation results demonstrate that the proposed control strategy significantly improves power allocation accuracy, maintains bus voltage and system frequency stability, and enables differential voltage and power adjustments under varying operating conditions. This effectively enhances the system's dynamic performance and transient stability. The study focuses on three DGs connected in parallel to a common AC bus with an unbalanced load. Future work will extend this research to microgrids with multiple DGs, considering the output characteristics of various DGs and refining the algorithm to improve the control strategy's performance in more complex experimental environments.

Acknowledgment

The authors would like to thanks for financial support and research facilities from Universiti Malaysia Perlis and the Malaysian Ministry of Higher Education (MOHE) through the Fundamental Research Grant Scheme (FRGS), (No: FRGS/1/2022/TK08/UNIMAP/02/51).

References

[1] R. H. Lasseter, "MicroGrids," in *2002 IEEE Power Engineering Society Winter Meeting. Conference Proceedings (Cat. No.02CH37309)*, 2002, pp. 305–308 vol.1.

[2] M. H. Saeed, W. Fangzong, B. A. Kalwar, and S. Iqbal, "A Review on Microgrids' Challenges Perspectives," *IEEE Access*, vol. 9. Institute of Electrical and Electronics Engineers Inc., pp. 166502–166517, 2021.

[3] M. S. Hossain, M. A. Hasan, N. A. M. Said, W. A. Halim, and A. Jidin, "Reduced Device Count Multilevel Inverter Topology for Renewable Energy Applications: A Brief Review," in 2023 IEEE Conference on Energy Conversion (CENCON), 2023, pp. 41–46.

[4] M. Dashtdar, M. S. Nazir, S. M. S. Hosseinimoghadam, M. Bajaj, and S. Goud B, "Improving the Sharing of Active and Reactive Power of the Islanded Microgrid Based on Load Voltage Control," *Smart Science*, vol. 10, no. 2, pp. 142–157, Apr. 2022.

[5] Z. Quan and Y. W. Li, "Impact of PWM Schemes on the Common-Mode Voltage of Interleaved Three-Phase Two-Level Voltage Source Converters," *IEEE Transactions on Industrial Electronics*, vol. 66, no. 2, pp. 852–864, 2019.

[6] M. Castilla, M. Velasco, J. Miret, Á. Borrell, and R. Guzmán, "Control Scheme for Negative-Sequence Voltage Compensation and Current Sharing in Inverter-Based Grid-Connected Microgrids," *IEEE Trans Power Electron*, vol. 37, no. 6, pp. 6556–6567, 2022.

[7] Z. Liu, S. Miao, Z. Fan, J. Liu, and Q. Tu, "Improved power flow control strategy of the hybrid AC/DC microgrid based on VSM," *IET Generation, Transmission & Distribution*, vol. 13, no. 1, pp. 81–91, Jan. 2019.

[8] M. Baharizadeh, H. R. Karshenas, and J. M. Guerrero, "An improved power control strategy for hybrid AC-DC microgrids," *International Journal of Electrical Power & Energy Systems*, vol. 95, pp. 364–373, 2018.

[9] X. Hu, Z.-W. Liu, G. Wen, X. Yu, and C. Liu, "Voltage Control for Distribution Networks via Coordinated Regulation of Active and Reactive Power of DGs," *IEEE Trans Smart Grid*, vol. 11, no. 5, pp. 4017–4031, 2020.

[10] M. Gheisarnejad, H. Mohammadi-Moghadam, J. Boudjadar, and M. H. Khooban, "Active Power Sharing and Frequency Recovery Control in an Islanded Microgrid With Nonlinear Load and Nondispatchable DG," *IEEE Syst J*, vol. 14, no. 1, pp. 1058–1068, 2020.

[11] S. Iqbal *et al.*, "Aggregation of EVs for Primary Frequency Control of an Industrial Microgrid by Implementing Grid Regulation & Charger Controller," *IEEE Access*, vol. 8, pp. 141977–141989, 2020.

[12] P. Quintana-Barcia, T. Dragicevic, J. Garcia, J. Ribas, and J. M. Guerrero, "A Distributed Control Strategy for Islanded Single-Phase Microgrids with Hybrid Energy Storage Systems Based on Power Line Signaling," *Energies (Basel)*, vol. 12, no. 1, 2019.

[13] C. Andalib-Bin-Karim, X. Liang, and H. Zhang, "Fuzzy-Secondary-Controller-Based Virtual Synchronous Generator Control Scheme for Interfacing Inverters of Renewable Distributed Generation in Microgrids," *IEEE Trans Ind Appl*, vol. 54, no. 2, pp. 1047–1061, 2018.

[14] K. Yu, Q. Ai, S. Wang, J. Ni, and T. Lv, "Analysis and Optimization of Droop Controller for Microgrid System Based on Small-Signal Dynamic Model," *IEEE Trans Smart Grid*, vol. 7, no. 2, pp. 695–705, 2016.

[15] L. Zhang, H. Zheng, Q. Hu, B. Su, and L. Lyu, "An Adaptive Droop Control Strategy for Islanded Microgrid Based on Improved Particle Swarm Optimization," *IEEE Access*, vol. 8, pp. 3579–3593, 2020.

[16] X. Leng *et al.*, "Adaptive Droop Control Strategy for Island Microgrid Based on Improved Particle Swarm Optimization Algorithm," in *Genetic and Evolutionary Computing*, S.-C. Chu, J. C.-W. Lin, J. Li, and J.-S. Pan, Eds., Singapore: Springer Nature Singapore, 2022, pp. 3–13.

[17] A. Milczarek, M. Malinowski, and J. M. Guerrero, "Reactive Power Management in Islanded Microgrid—Proportional Power Sharing in Hierarchical Droop Control," *IEEE Trans Smart Grid*, vol. 6, no. 4, pp. 1631–1638, 2015.

[18] M. C. Chandorkar, D. M. Divan, and R. Adapa, "Control of parallel connected inverters in standalone AC supply systems," *IEEE Trans Ind Appl*, vol. 29, no. 1, pp. 136–143, 1993.

[19] W. Yuan, Y. Wang, D. Liu, and F. Deng, "Adaptive Droop Control Strategy of Autonomous Microgrid for Efficiency Improvement," in *2019 IEEE 10th International Symposium on Power Electronics for Distributed Generation Systems (PEDG)*, 2019, pp. 972–977.

[20] W. Yuan, Y. Wang, D. Liu, F. Deng, and Z. Chen, "Efficiency-Prioritized Droop Control Strategy of AC Microgrid," *IEEE J Emerg Sel Top Power Electron*, vol. 9, no. 3, pp. 2936–2950, 2021, doi: 10.1109/JESTPE.2020.2967756.

[21] W. Yuan, Y. Wang, D. Liu, F. Deng, and Z. Chen, "Efficiency Modelling and Analysis of Multi-bus Microgrid with Transmission Network," in *2020 IEEE 9th International Power Electronics and Motion Control Conference (IPEMC2020-ECCE Asia)*, 2020, pp. 676–681.

[22] S. Cheng, H. Zhan, and Z. Shu, "An innovative hybrid multi-objective particle swarm optimization with or without constraints handling," *Appl Soft Comput*, vol. 47, pp. 370–388, 2016.

[23] Q. Feng *et al.*, "Multiobjective Particle Swarm Optimization Algorithm Based on Adaptive Angle Division," *IEEE Access*, vol. 7, pp. 87916–87930, 2019.

[24] "IGBT modules technical information, CM100TU-12H, Powerex datasheet, 2009."

[25] "IGBT modules technical information, FS200R07PE4, Infineon datasheet, 2013."

[26] "IGBT modules technical information, FS225R12OE4, Infineon datasheet, 2013."